

A bright gamma-ray flare interpreted as a giant magnetar flare in NGC 253

D. Svinkin¹, D. Frederiks¹, K. Hurley², R. Aptekar¹, S. Golenetskii¹, A. Lysenko¹, A.V. Ridnaia¹, A. Tsvetkova¹, M. Ulanov¹, T.L. Cline^{3,*}, I. Mitrofanov⁴, D. Golovin⁴, A. Kozyrev⁴, M. Litvak⁴, A. Sanin⁴, A. Goldstein⁵, M.S. Briggs⁶, C. Wilson-Hodge⁷, A. von Kienlin⁸, X.-L. Zhang⁸, A. Rau⁸, V. Savchenko⁹, E. Bozzo⁹, C. Ferrigno⁹, P. Ubertini¹⁰, A. Bazzano¹⁰, J.C. Rodi¹⁰, S. Barthelmy³, J. Cummings¹¹, H. Krimm¹², D.M. Palmer¹³, W. Boynton¹⁴, C.W. Fellows¹⁴, K.P. Harshman¹⁴, H. Enos¹⁴, and R. Starr¹⁵

¹Ioffe Institute, 26 Politekhnicheskaya, St Petersburg, 194021, Russia

²Space Sciences Laboratory, University of California, 7 Gauss Way, Berkeley, CA 94720-7450, USA

³NASA Goddard Space Flight Center, Greenbelt, Maryland, USA

⁴Space Research Institute, 84/32 Profsoyuznaya, Moscow, 117997, Russia

⁵Science and Technology Institute, Universities Space Research Association, Huntsville, AL 35805, USA

⁶Space Science Department, University of Alabama in Huntsville, 320 Sparkman Drive, Huntsville, AL 35899, USA

⁷NASA Marshall Space Flight Center, Huntsville, AL 35812, USA

⁸Max-Planck-Institut für extraterrestrische Physik, Giessenbachstrasse 1, D-85748 Garching, Germany

⁹Department of Astronomy, University of Geneva, chemin d'Écogia 16, 1290, Versoix, Switzerland

¹⁰INAF – Institute for Space Astrophysics and Planetology, Via Fosso del Cavaliere 100, Roma, Italy

¹¹Center for Astrophysical Sciences, Johns Hopkins University, Baltimore, MD, USA

¹²National Science Foundation, Alexandria, VA 22314, USA

¹³Los Alamos National Laboratory, B244, Los Alamos, NM 87545, USA

¹⁴Lunar and Planetary Laboratory, University of Arizona, Tucson, AZ, USA

¹⁵Catholic University of America, Washington, DC 20064, USA

*Retired

ABSTRACT

Magnetars^{1–3} are young, highly magnetized neutron stars that produce extremely rare giant flares of gamma-rays, the most luminous astrophysical phenomena in our Galaxy. The detection of these flares from outside the Local Group of galaxies has been predicted^{4,5}, with just two candidates

so far^{6–10}. Here we report on the extremely bright gamma-ray flare GRB 200415A of April 15, 2020, which we localize, using the Interplanetary Network, to a tiny (20 sq. arcmin) area on the celestial sphere, that overlaps the central region of the Sculptor galaxy at ~ 3.5 Mpc from the Milky Way. From the *Konus-Wind* detections, we find a striking similarity between GRB 200415A and GRB 051103, the even more energetic flare that presumably originated from the M81/M82 group of galaxies at nearly the same distance (3.6 Mpc). Both bursts display a sharp, millisecond-scale, hard-spectrum initial pulse, followed by an approximately 0.2 s long steadily fading and softening tail. Apart from the huge initial pulses of magnetar giant flares, no astrophysical signal with this combination of temporal and spectral properties and implied energy has been reported previously. At the inferred distances, the energy released in both flares is on par with that of the December 27, 2004 superflare^{4,11,12} from the Galactic magnetar SGR 1806–20, but with a higher peak luminosity. Taken all together, this makes GRB 200415A and its twin GRB 051103 the most significant candidates for extragalactic magnetar giant flares, both a factor of $\gtrsim 5$ more luminous than the brightest Galactic magnetar flare observed previously, thus providing an important step towards a better understanding of this fascinating phenomenon.

MAIN TEXT

Magnetars^{2,3} are a special rare class of neutron stars with strong magnetic fields¹ ($B \sim 10^{14} - 10^{15}$ G). Some magnetars (or Soft-Gamma Repeaters, SGRs) exhibit bursting emission in hard X-rays/soft gamma-rays. During the active stage, which may last from several days to years, SGRs emit randomly occurring short (from milliseconds to seconds long) hard X-ray bursts with peak luminosities of $\sim 10^{38} - 10^{42}$ erg s⁻¹. Much more rarely, perhaps several times during the SGR stage¹¹, assumed to last up to $\sim 10^5$ years which corresponds to the SGR magnetic field decay time-scale, a magnetar may emit a giant flare (GF) with the sudden release of an enormous amount of energy in the form of gamma-rays $\sim (0.01 - 1) \times 10^{46}$ erg. A GF displays a short (fraction of a second) initial pulse of radiation with a sharp rise and a more shallow decay which evolves into a soft spectrum, long-duration decaying tail modulated with the neutron star rotation period. Only a dozen burst-emitting magnetars in our Galaxy and Large Magellanic Cloud are known so far and only three of them produced a GF during the active stage¹³. Due to the enormous luminosity of the

initial pulse, GFs can be detected from magnetars in nearby galaxies up to tens of megaparsecs away^{4,5}. In this case, the initial pulse may mimic a short gamma-ray burst (GRB) produced by the merger of a binary compact object (two neutron stars or a neutron star and a black hole) in galaxies at cosmological distances. Neither the rotationally modulated tail, nor the short weaker X-ray bursts preceding and following a GF can be observed even from nearby galaxies by the current wide-field gamma-ray monitors. **Thus, the main evidence supporting the magnetar nature of such bursts are spatial coincidence with a galaxy, consistency of the burst light curve and energetics with known GFs, and non-detection of a gravitational wave signal indicative of a short GRB.** Up to now only two short GRBs were proposed to be magnetar giant flares outside our Galaxy and its satellites (extragalactic magnetar GFs, eMGFs): GRB 051103, associated with the M81/M82 group of galaxies^{6–8} at a distance $D_{\text{M81/M82}} = 3.6 \text{ Mpc}$ ¹⁴ and GRB 070201, in the Andromeda galaxy (M31)^{9,10} at $D_{\text{M31}} = 0.77 \text{ Mpc}$ ¹⁵. Detailed searches for GFs from nearby galaxies have not revealed any other credible candidates^{16,17} and put an upper limit on the fraction of GFs in the short GRB population less than $\sim 10\%$.

On 15 April 2020 the extremely bright, short GRB 200415A occurred at 08:48:06 UT at the Earth, and was detected by five missions of the Interplanetary network of gamma-ray detectors (IPN, see Methods). We report here the final $\sim 20 \text{ arcmin}^2$ burst localisation by the IPN (see Methods), which overlaps the central part of the nearby Sculptor galaxy, also designated as NGC 253, at a distance $D_{\text{NGC253}} = 3.5 \text{ Mpc}$ ¹⁸ (Figure 1). The chance occurrence for GRB 200415A to be spatially consistent with a nearby galaxy likely to produce detectable eMGFs is approximately 1 in 200000¹⁹.

A preliminary analysis of the *Konus-Wind* (KW) detection²⁰ of GRB 200415A revealed a remarkable similarity between this burst and GRB 051103, historically the first eMGF candidate. To explore this similarity further, we performed a detailed comparative study of their temporal and spectral properties (Methods); the results are in general agreement with those previously reported on the latter event^{7,8}.

As observed by KW, the 2 ms light curves of GRB 200415A and GRB 051103 start with the fast, ($\sim 2 \text{ ms}$) rise of a narrow ($\sim 4 \text{ ms}$) initial pulse (IP), which is followed by an exponentially decaying phase with count-rate e-folding time $\tau_{\text{cr}} \sim 50 \text{ ms}$ (Figure 2). The total burst durations are 0.138 s (GRB 200415A) and 0.324 s (GRB 051103), and the values of T_{90} (the duration of the time interval which contains the central 90% of the total burst count fluence) are $0.100 \pm 0.014 \text{ s}$ and $0.138 \pm 0.005 \text{ s}$, respectively (hereafter

all the quoted uncertainties are at the 68% confidence level). Although the peak count rates, reached in the first 2 ms of the IPs, are very similar, $\sim (1.5\text{--}1.7) \times 10^5 \text{ s}^{-1}$, the photon flux over the entire extent of the decaying phase is about twice as high in GRB 051103 as in GRB 200415A.

The burst hardness (the ratio between the 390–1600 keV and 90–390 keV count rates) rapidly increases during the initial pulses, peaks during the following ~ 8 ms, and then gradually decays with the burst count rate. Our spectral analysis (Methods) shows that starting from the rise of the IP and up to $\sim T_0 + 100$ ms, the energy spectra of both bursts are well described by a cut-off power law function (CPL; $\propto E^\alpha \exp(-E(\alpha + 2)/E_p)$). The temporal evolution of the spectra is illustrated in Figure 2 which shows the behaviour of the CPL model parameters: the peak energy of the $EF(E)$ spectrum E_p (panel **c**) and photon power-law index α (panel **d**). The initial narrow pulses of both bursts are characterized by $E_p \sim 1.2$ MeV, with $\alpha \sim -0.6$ for GRB 200415A and a much harder $\alpha \sim -0.1$ for GRB 051103. This E_p was the highest reached in the entire event for GRB 200415A, while the hardest emission in GRB 051103 ($E_p \sim 3$ MeV, $\alpha \sim 0.2$) was reached during the subsequent ~ 30 ms. A non-thermal CPL model, with E_p decaying nearly exponentially, adequately describes burst spectra up to $\sim T_0 + 100$ ms. Afterwards, the very hard photon index α becomes poorly constrained and, simultaneously, the emission spectrum can be described by a blackbody function (with a temperature $kT \sim 70\text{--}100$ keV), which is excluded by our analysis at the initial stages of the bursts.

Panel **b** of Figure 2 shows the temporal evolution of the 20 keV–10 MeV energy flux. For both bursts, the flux peaks in the initial spike and, starting from $\sim T_0 + 50$ ms, decays with $\tau_{\text{flux}} \sim 30$ ms. In accordance with the burst similarities in peak count rate and energy spectrum, measured in the IPs, their 4 ms peak flux estimates also agree within errors: $0.96^{+0.32}_{-0.16} \times 10^{-3} \text{ erg cm}^{-2} \text{ s}^{-1}$ and $1.15^{+0.52}_{-0.24} \times 10^{-3} \text{ erg cm}^{-2} \text{ s}^{-1}$ for GRB 200415A and GRB 051103, respectively.

The time-integrated spectra of both flares, measured from T_0 to $T_0 + 0.192$ s, are best described by a sum of non-thermal (CPL) and thermal (BB) components. The burst 20 keV–10 MeV fluences are $8.5^{+1.2}_{-1.0}$ ($34.3^{+4.0}_{-2.0}$) $\times 10^{-6} \text{ erg cm}^{-2}$ for GRB 200415A (GRB 051103), with blackbody component contributions of $\sim 14\%$ and $\sim 9\%$, respectively. The contribution of the initial short spike to the total burst fluence is about 45% for GRB 200415A, and just 13% for GRB 051103.

Thus, the extremely bright short GRB 200415A, which strong evidence suggests is associated with

the Sculptor galaxy, is strikingly similar to GRB 051103, that presumably originated from the M81/M82 group of galaxies at nearly the same distance, in terms of light curve morphology, spectral behavior, and observed peak energy flux. A lightcurve with a bright, millisecond scale initial pulse followed by an exponentially decaying emission is quite unusual for short cosmological GRBs; none of $\gtrsim 500$ short bursts detected by *Konus-Wind* in more than 25 years of observations displays such a shape^{?,21}. On the other hand, this pattern was observed in two Galactic magnetar giant flares, from SGR 1900+14^{22,23} and SGR 1806-20^{23,24}. Furthermore, higher time resolution light curves of GRB 200415A from *Swift*-BAT and *Fermi*-GBM²⁵ show an initial short (< 1 ms) sub-peak, followed by a sharp decrease for ~ 1 ms, before the main part of the peak. This pattern is also seen in the SGR 1806-20 giant flare¹¹ and may be a general property of magnetar GFs that can be used to identify them within the short GRB sample. Thus, the interpretation of both GRB 200415A and GRB 051103 as magnetar giant flares is strongly suggested, with additional support from the non-detection of an accompanying gravitational wave signal for GRB 051103²⁶ (there is no sensitive coverage by a gravitational wave detector for GRB 200415A).

At source distances $D_{\text{NGC253}} = 3.5$ Mpc and $D_{\text{M81}} = 3.6$ Mpc, the characteristic radius of the emission region, estimated from the blackbody spectral fits, is $R \sim 20 - 40$ km, of the same order as the radius of a neutron star or its magnetosphere. The implied isotropic-equivalent energy release in γ -rays, E_{iso} , is ~ 1.3 (~ 5.3) $\times 10^{46}$ erg, and the isotropic-equivalent peak luminosity, L_{iso} , is ~ 1.4 (~ 1.8) $\times 10^{48}$ erg s⁻¹ for GRB 200415A (GRB 051103). Thus, the total energies released in both flares are comparable with that estimated for the most energetic flare from a Galactic magnetar $\sim 2.3 \times 10^{46}$ erg⁹, but at much higher peak luminosity. Taken all together, this makes GRB 200415A and its twin GRB 051103 the most significant candidates for extragalactic magnetar giant flares, both a factor of $\gtrsim 5$ more luminous than any Galactic magnetar flare observed previously⁹. Assuming the same spectra and energetics, similar events can be detected with KW from distances up to ~ 16 Mpc. The properties of GRB 200415A and GRB 051103 are summarized in Extended Data Table 1.

Despite the strong evidence in favor of the magnetar GF nature of GRB 200415A and GRB 051103, it cannot completely be ruled out that they might belong to an as-yet undiscovered branch of the cosmological short GRB population. For the observed energy fluence, and assuming a cosmological redshift z of 0.05–1, GRB 200415A is consistent with the *Konus-Wind* sample of short GRBs with known redshifts^{27,28} in

terms of a hardness-intensity relation in the cosmological rest frame (see Extended Data Figure 1). In the case of GRB 051103, the implied short GRB redshift is $z \sim 1$, and intrinsic $E_p \sim 5$ MeV.

GRB 200415A, detected in the wide energy range ~ 10 keV up to GeV, by multiple space-based observatories, is to date the most comprehensively studied initial phase of MGF (the pulsating tail is beyond the sensitivity of current instruments from 3.5 Mpc⁸). The detection of extragalactic magnetar giant flares facilitates the study of emission processes on millisecond and sub-millisecond time scales²⁵ inaccessible to galactic events, which saturate almost all gamma-ray detectors. On the time scale accessible to KW ($\gtrsim 2$ ms), the single-peaked GRB 200425A and GRB 051103 are clearly different from the third known eMGF candidate, GRB 070201⁹, with a highly variable emission during the first ~ 50 ms. This suggests that the physical processes behind the emission in MGF initial pulses may develop on temporal scales spanning more than an order of magnitude. The exponential decay in both the flux and E_p is also observed in the GBM/BAT with higher statistical quality, which is used to interpret the physical emission process and environment of the likely neutron star progenitor²⁵. The recognition of GRB 200425A as an eMGF in the Sculptor galaxy has provided a clue for the interpretation of the delayed GeV photons detected by *Fermi*-LAT as the emission from interaction of a magnetar ultra-relativistic outflow with environmental gas²⁹. Finally, the detection and the subsequent retrospective eMGF search¹⁹ provide an excellent proxy for the magnetar population in nearby galaxies.

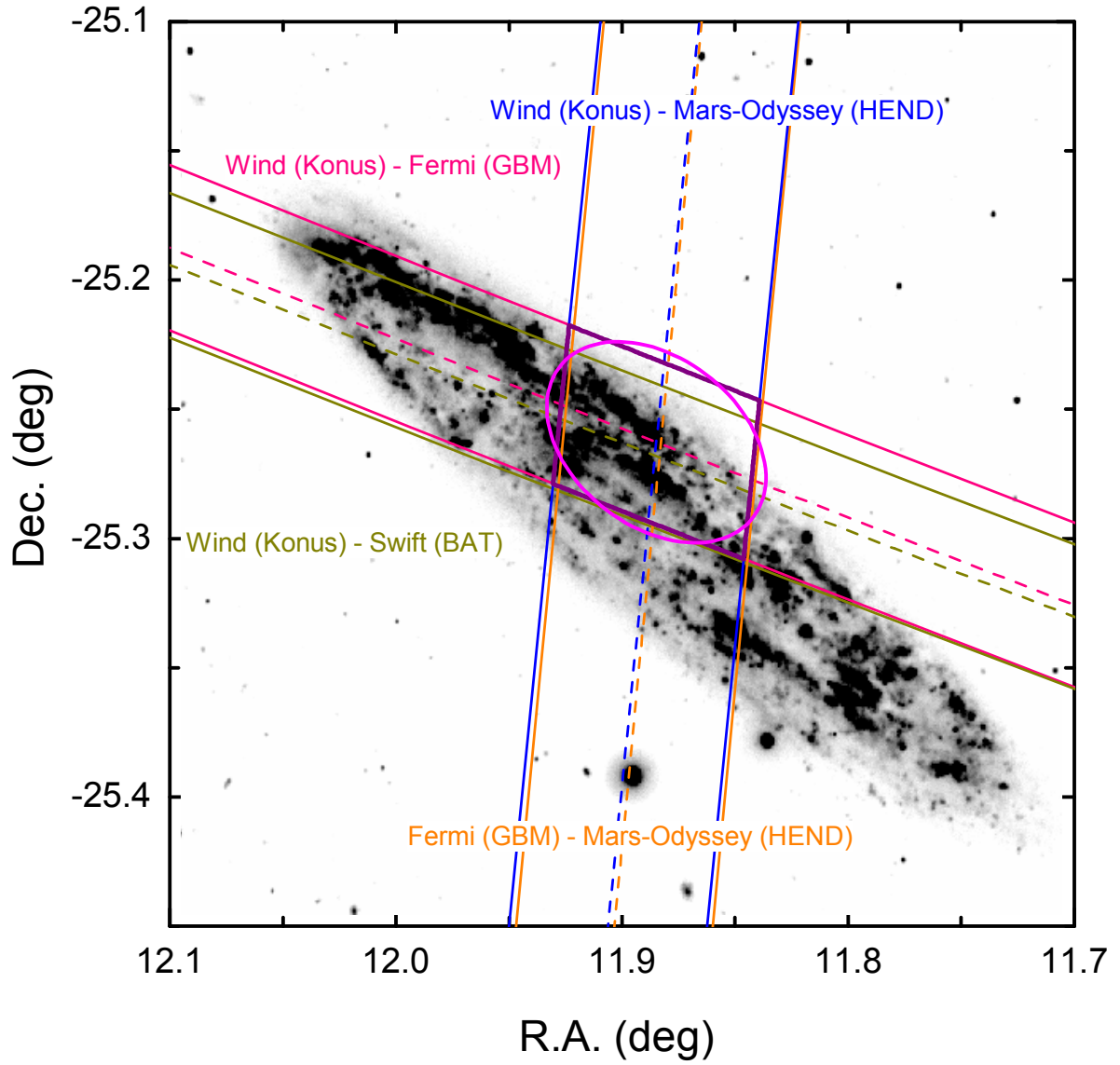


Figure 1. The final IPN localization of GRB 200415A superimposed on an image of the Sculptor galaxy from the GALEX survey (1750–2800 Å; see Methods). The localization is defined by the 4.73 arcmin wide *Wind-Odyssey* and 3.58 arcmin wide *Wind-Fermi* annuli. The IPN error box (purple parallelogram) is shown along with the 20 arcmin² 3σ error ellipse (shown in magenta) for the position. The coordinates are J2000.

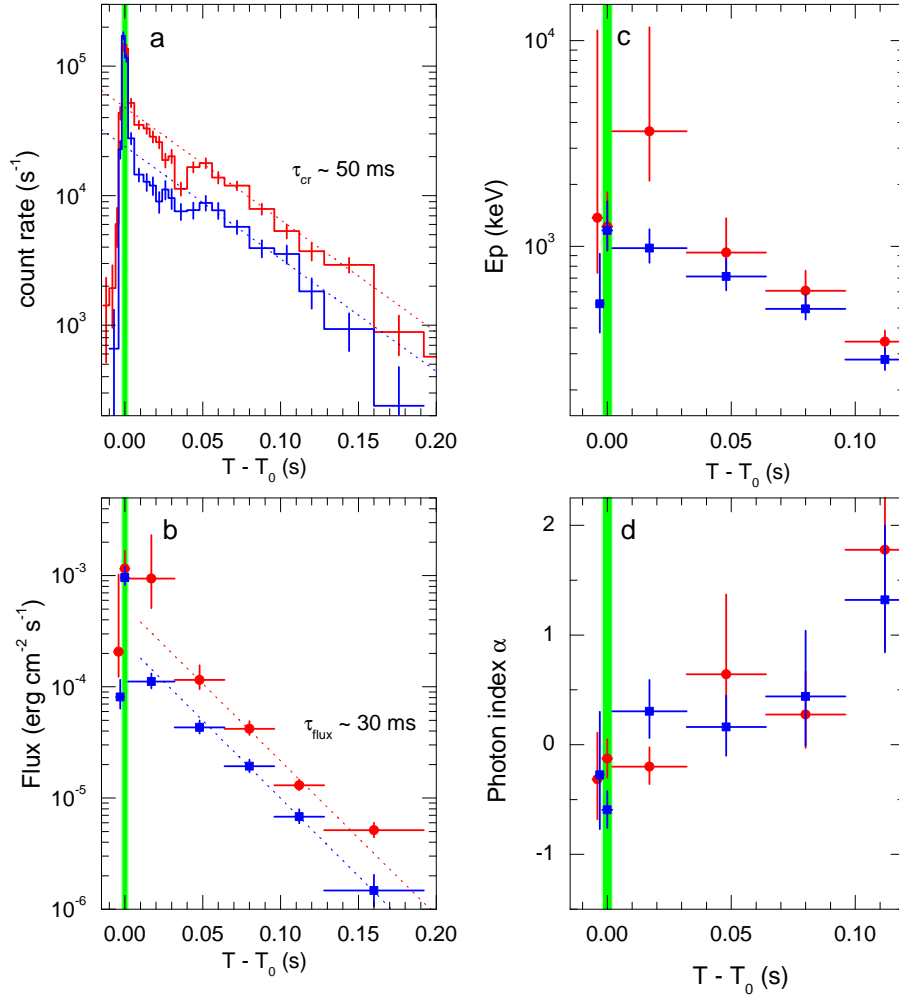


Figure 2. Time histories of the twin GRB 051103 (red) and GRB 200415A (blue) and evolution of their spectral parameters. All times are given relative to the KW trigger time T_0 . Panel **a** shows the burst time histories as recorded by *Konus-Wind*. Both events start with a sharp rise of an exceptionally bright, narrow (4 ms) initial pulse (IP), whose time interval is indicated by a green shaded area in each panel, followed by an exponential decay with $\tau_{\text{cr}} \sim 50$ ms (dotted lines). Panel **b** shows the evolution of the 20 keV–10 MeV energy flux, which, in both cases, peaks in the IP and, starting from $\sim T_0 + 50$ ms, decays with $\tau_{\text{flux}} \sim 30$ ms. The temporal evolution of the emission spectra is illustrated with the behavior of CPL model best-fit parameters: peak energy E_p (panel **c**) and photon power-law index α (panel **d**). Both bursts are characterized by $E_p \sim 1.2$ MeV in the IP, which is the hardest part of GRB 200415A, while the hardest emission in GRB 051103 (with $E_p \sim 3$ MeV) was detected during the subsequent ~ 30 ms. A non-thermal CPL model adequately describes burst spectra up to $\sim T_0 + 100$ ms; afterwards, the hard power-law photon index α becomes poorly constrained and, simultaneously, the emission spectrum can be described by a blackbody function with $kT \sim 70$ –100 keV. Vertical error bars indicate 68% confidence intervals, and horizontal error bars indicate the duration of the interval.

References

1. Duncan, R. C. & Thompson, C. Formation of Very Strongly Magnetized Neutron Stars: Implications for Gamma-Ray Bursts. *Astrophys. J.* **392**, L9 (1992).
2. Mereghetti, S. *et al.* Magnetars: Properties, Origin and Evolution. *Space Sci. Rev.* **191**, 315-338 (2015). [1503.06313](#).
3. Kaspi, V. M. & Beloborodov, A. M. Magnetars. *ARA&A* **55**, 261-301 (2017). [1703.00068](#).
4. Hurley, K. *et al.* An exceptionally bright flare from SGR 1806-20 and the origins of short-duration γ -ray bursts. *Nature* **434**, 1098-1103 (2005). [astro-ph/0502329](#).
5. Popov, S. B. & Stern, B. E. Soft gamma repeaters outside the Local Group. *Mon. Not. R. Astron. Soc.* **365**, 885-890 (2006). [astro-ph/0503532](#).
6. Ofek, E. O. *et al.* The Short-Hard GRB 051103: Observations and Implications for Its Nature. *Astrophys. J.* **652**, 507-511 (2006). [astro-ph/0609582](#).
7. Frederiks, D. D. *et al.* On the possibility of identifying the short hard burst GRB 051103 with a giant flare from a soft gamma repeater in the M81 group of galaxies. *Astronomy Letters* **33**, 19-24 (2007). [astro-ph/0609544](#).
8. Hurley, K. *et al.* A new analysis of the short-duration, hard-spectrum GRB 051103, a possible extragalactic soft gamma repeater giant flare. *Mon. Not. R. Astron. Soc.* **403**, 342-352 (2010). [0907.2462](#).
9. Mazets, E. P. *et al.* A Giant Flare from a Soft Gamma Repeater in the Andromeda Galaxy (M31). *Astrophys. J.* **680**, 545-549 (2008). [0712.1502](#).
10. Ofek, E. O. *et al.* GRB 070201: A Possible Soft Gamma-Ray Repeater in M31. *Astrophys. J.* **681**, 1464-1469 (2008). [0712.3585](#).
11. Palmer, D. M. *et al.* A giant γ -ray flare from the magnetar SGR 1806 - 20. *Nature* **434**, 1107-1109 (2005). [astro-ph/0503030](#).

12. Frederiks, D. D. *et al.* Giant flare in SGR 1806-20 and its Compton reflection from the Moon. *Astronomy Letters* **33**, 1-18 (2007). [astro-ph/0612289](#).
13. Olausen, S. A. & Kaspi, V. M. The McGill Magnetar Catalog. *Astrophys. J. Supp.* **212**, 6 (2014). [1309.4167](#).
14. Karachentsev, I. D. & Kashibadze, O. G. Masses of the local group and of the M81 group estimated from distortions in the local velocity field. *Astrophysics* **49**, 3-18 (2006).
15. Karachentsev, Igor D. *et al.* A Catalog of Neighboring Galaxies. *Astron. J.* **127**, 2031-2068 (2004).
16. Ofek, E. O. Soft Gamma-Ray Repeaters in Nearby Galaxies: Rate, Luminosity Function, and Fraction among Short Gamma-Ray Bursts. *Astrophys. J.* **659**, 339-346 (2007). [astro-ph/0611860](#).
17. Svinkin, D. S. *et al.* A search for giant flares from soft gamma-ray repeaters in nearby galaxies in the Konus-WIND short burst sample. *Mon. Not. R. Astron. Soc.* **447**, 1028-1032 (2015). [1411.5589](#).
18. Rekola, R. *et al.* Distance to NGC 253 based on the planetary nebula luminosity function. *Mon. Not. R. Astron. Soc.* **361**, 330-336 (2005).
19. Burns, E. *et al.* Identification of a local sample of gamma-ray bursts consistent with a magnetar giant flare origin. *Accepted for publication in ApJL* (2021).
20. Frederiks, D. *et al.* Konus-Wind observation of GRB 200415A (a magnetar Giant Flare in Sculptor Galaxy?). *GRB Coordinates Network* **27596**, 1 (2020).
21. Svinkin, D. S. *et al.* The Second Konus-Wind Catalog of Short Gamma-Ray Bursts. *Astrophys. J. Supp.* **224**, 10 (2016). [1603.06832](#).
22. Aptekar, R. L. *et al.* Konus Catalog of Soft Gamma Repeater Activity: 1978 to 2000. *Astrophys. J. Supp.* **137**, 227-277 (2001). [astro-ph/0004402](#).
23. Tanaka, Y. T. *et al.* Comparative Study of the Initial Spikes of Soft Gamma-Ray Repeater Giant Flares in 1998 and 2004 Observed with Geotail: Do Magnetospheric Instabilities Trigger Large-Scale Fracturing of a Magnetar's Crust?. *Astrophys. J.* **665**, L55-L58 (2007). [0706.3123](#).
24. Terasawa, T. *et al.* Repeated injections of energy in the first 600ms of the giant flare of SGR1806 - 20. *Nature* **434**, 1110-1111 (2005). [astro-ph/0502315](#).

25. Roberts, O. J. *et al.* Rapid Spectral Variability of a Giant Flare from an Extragalactic Magnetar. *Accepted for publication in Nature* (2021).
26. Abadie, J. *et al.* Implications for the Origin of GRB 051103 from LIGO Observations. *Astrophys. J.* **755**, 2 (2012). [1201.4413](#).
27. Pozanenko, A. *et al.* GRB 200415A (possible magnetar Giant Flare in Sculptor Galaxy): INTEGRAL observations. *GRB Coordinates Network* **27627**, 1 (2020).
28. Tsvetkova, A. *et al.* The Konus-Wind Catalog of Gamma-Ray Bursts with Known Redshifts. I. Bursts Detected in the Triggered Mode. *Astrophys. J.* **850**, 161 (2017). [1710.08746](#).
29. The Fermi LAT Collaboration High-Energy Emission from a Magnetar Giant Flare in the Sculptor Galaxy. *Accepted for publication in Nature Astronomy* (2021).

Methods

Observations

GRB 200415A occurred at 08:48:06 UT at the Earth, and was detected by the Gamma-ray burst monitor (GBM) on-board the *Fermi* Gamma-ray Space Telescope Mission³⁰ and the Burst Alert Telescope (BAT, outside the coded field of view) on-board the Neil Gehrels *Swift* Observatory³¹ in low Earth orbits; the SPI telescope anticoincidence system³² (SPI-ACS) and Pixellated Imaging Caesium Iodide Telescope^{33,34} (IBIS-PICsIT) instruments on-board the International Gamma-Ray Astrophysics Laboratory (*INTEGRAL*) in an eccentric Earth orbit at 0.44 light seconds from Earth; the *Mars-Odyssey* High Energy Neutron Detector^{35,36} (HEND) in orbit around Mars at 672 lt-s from Earth; the Konus-*Wind*³⁷ (KW) gamma-ray spectrometer on the *Wind* mission³⁸ in a Lissajous orbit at the L_1 libration point of the Sun-Earth system at a distance of 4.8 lt-s; and the Modular X- and Gamma-Ray Sensor (MXGS) of The Atmosphere-Space Interactions Monitor ASIM³⁹ on-board the *International Space Station* (not a part of the IPN).

Two independent and consistent *Fermi*-GBM localizations^{40,41} RoboBA⁴² and BALROG^{43,44} were announced in GCN Circulars at 08:58 UT and 09:11 UT, respectively, each with 3σ probability region covering more than 1000 deg^2 . Exploiting the difference in the arrival time of the gamma-ray signals at the four Interplanetary Network (IPN, see the next section) instruments (GBM, BAT, HEND, and SPI-ACS), a preliminary 1.5 deg^2 IPN error box was announced at 16:51 UT⁴⁵, where it was pointed out that this event might be a magnetar GF in the Sculptor galaxy (NGC 253) located at $D_{\text{NGC253}} = 3.5 \text{ Mpc}$. The *Fermi*-LAT localization, announced at 19:30 UT⁴⁶ was consistent with the box.

As soon as Konus-*Wind* data arrived the improved 274 arcmin^2 box (~ 20 times smaller than the initial box) was published on 16 April 16:16 UT⁴⁷ which strengthened the association of the burst with the galaxy. The box was close to the 68% confidence contours of the updated *Fermi*-LAT localization⁴⁸, published on 16 April 20:48 UT. The IPN localization was within about 37 deg of the Sun, making X-ray and optical follow-up observations challenging. The only optical observation of the Sculptor galaxy, resulting in an upper limit, was reported by the MASTER telescope network on 17 April⁴⁹.

Interplanetary network The Interplanetary network (IPN; <http://www.ssl.berkeley.edu/ipn3/>) is a group of spacecraft orbiting the Earth and Mars equipped with gamma-ray burst detectors used to localize gamma-ray bursts⁵⁰. When a GRB arrives at two spacecraft, it may be localized (triangulated) to an annulus on the sky, determined by the measured propagation time delay and spacecraft positions. Three spacecraft produce two possible locations (IPN error boxes). The ambiguity can be eliminated by the addition of a fourth, non-coplanar spacecraft, by the anisotropic response of KW, or by the GBM localization⁵¹.

The propagation time delay and its uncertainty are calculated by cross-correlation⁵². The systematic uncertainties are estimated using the comparison of IPN triangulations with precise GRB positions⁵¹.

The declared on-board clock accuracy of the spacecraft are: down to 1 μ s for *Fermi*; ~ 200 μ s for *Swift*; $\lesssim 1$ ms for *Wind*; ~ 100 μ s for INTEGRAL; for *Mars-Odyssey* an overall 3σ systematic uncertainty which includes timing and other effects derived from IPN observations of precisely localized GRBs is better than 360 ms. The *Wind* clock drift information is provided at https://pwgdata.sci.gsfc.nasa.gov/pub/wind_clock/.

Near-Earth spacecraft ephemerides are derived from two-line elements (TLE) available at <https://www.space-track.org> using SGP8 model. The *Wind* predicted ephemerides data and their description are available at https://spdf.gsfc.nasa.gov/pub/data/wind/orbit/pre_or/ and https://cdaweb.gsfc.nasa.gov/misc/NotesW.html#WI_OR_PRE, respectively. *Mars-Odyssey* ephemerides were taken from JPL's HORIZONS system <https://ssd.jpl.nasa.gov/horizons.cgi>

For the near-Earth spacecraft and *Wind*, ephemeris uncertainties contribute less than 1 ms to the propagation time delay, so we conservatively assume a systematic error in Konus-GBM and Konus-BAT triangulations to be 1 ms. For the Konus-HEND and GBM-HEND triangulations we take 360 ms as the 3σ systematic uncertainty.

For GRB 200415A triangulation we used the following lightcurves: 2 ms Konus (see Konus-Wind section), 390-1600 keV; 0.1 ms GBM, 360-1000 keV, constructed from the TTE data of triggered detectors (0, 1, 2, 3, 4, 5, 9, and a; only NaI data were used); 0.1 ms BAT, 25-350 keV, constructed from the TTE data from the GUANO system⁵³; 250 ms HEND, 50-3000 keV; and 7.8 ms INTEGRAL-PICsIT,

Methods Table 1. Triangulation annuli: the instruments involved in triangulation and the lightcurve temporal resolution used (1st column), the annulus center right ascension and declination in the equatorial J2000 system (2nd and 3rd columns, respectively), the annulus radius (4th column), and its half width corresponding to 3σ statistical cross-correlation time delay uncertainty with systematics added in quadrature.

Instruments involved	R.A. (J2000) (deg)	Dec.(J2000) (deg)	R (deg)	δR (deg)
GBM(0.1 ms)–KW(2 ms)	1.9406	2.0665	28.9781	0.0298
BAT(0.1 ms)–KW(2 ms)	2.0920	2.0554	28.9243	0.0262
KW(2 ms)–HEND(250 ms)	313.0127	-18.9203	54.5051	0.0394
GBM(1 ms)–HEND(250 ms)	313.3351	-18.8199	54.2444	0.0391
KW(2 ms)–PICsIT(7.8 ms)	4.1624	-2.1891	24.2751	0.1681

250-2000 keV.

Using these data we derived five annuli (Methods Table 1). The final IPN 3σ box was constructed from Konus-GBM and Konus-HEND annuli (Methods Table 2). We used the Konus-GBM annulus instead of the narrower Konus-BAT one due to the similarity of the two instruments’ energy bands. GBM saturation occurred near the burst peak and does not significantly affect the cross-correlation with the Konus 2 ms resolution light curve.

The annuli were combined to yield an error ellipse⁵⁴, with a major axis corresponding to the Konus-GBM annulus, and a minor axis corresponding to the Konus-HEND annulus. We obtain a 3σ error ellipse centred at R.A.(J2000) = 11.885 deg, Dec.(J2000) = -25.263 deg with major and minor axes 6.25 and 4.07 arcmin, respectively, and position angle of 61.135 deg. The ellipse area is 20 arcmin².

The ellipse contains the central part of the Sculptor galaxy (NGC 253; Figure 1). The image was obtained with the Galaxy Evolution Explorer *GALEX*⁵⁵ during the *GALEX* Nearby Galaxies Survey⁵⁶ (Observation ID: 2482083865531777024). The NGC 253 image was obtain via MAST portal (<https://mast.stsci.edu>).

Konus-Wind

Konus-Wind³⁷ (KW) consists of two identical NaI(Tl) scintillation detectors, each with 2π sr field of view, mounted on opposite faces of the rotationally stabilized *Wind* spacecraft³⁸, such that one detector (S1)

Methods Table 2. The 3σ IPN box: The error box area is 17 sq. arcmin, and its maximum (minimum) dimensions are 7 arcmin (4 arcmin). The Sun distance was ~ 37 deg.

Box center/ vertices	R.A. (J2000) (deg)	Dec.(J2000) (deg)
Center	11.885 (00h 47m 32s)	-25.263 (-25d 15m 47s)
1	11.846 (00h 47m 23s)	-25.308 (-25d 18m 29s)
2	11.931 (00h 47m 43s)	-25.279 (-25d 16m 44s)
3	11.923 (00h 47m 42s)	-25.218 (-25d 13m 05s)
4	11.839 (00h 47m 21s)	-25.247 (-25d 14m 49s)

points towards the south ecliptic pole, thereby observing the south ecliptic hemisphere, while the other (S2) observes the north ecliptic hemisphere.

Each KW detector is a cylinder 5 inches in diameter and 3 inches in height, placed into an aluminum container with a beryllium entrance window. The crystal scintillator is viewed by a photomultiplier tube through a 20 mm thick lead glass, which provides effective detector shielding from the spacecraft's background in the soft spectral range. The detector effective area is $\sim 80\text{--}160\text{ cm}^2$, depending on the photon energy and incident angle. The energy range of gamma-ray measurements covers the incident photon energy interval from 20 keV to 20 MeV.

The instrument has two operational modes: waiting and triggered. While in the waiting mode, the count rates (lightcurve) are recorded in three energy band covering the $\sim 20\text{--}1500$ keV energy band, see Methods Table 3, with 2.944 s time resolution. When the count rate in G2 exceeds a $\approx 9\sigma$ threshold above the background on one of two fixed time-scales, 1 s or 140 ms, the instrument switches into the triggered mode.

In the triggered mode, light curves are recorded in the same bands, starting from 0.512 s before the trigger time T_0 with time resolution varying from 2 ms up to 256 ms. For the bursts of interest here, the whole time history is available with 2 ms resolution.

Multichannel spectral measurements are carried out, starting from the trigger time T_0 (no multichannel spectra are available before T_0) in two overlapping energy intervals PHA1 and PHA2 (Methods Table 3). with 64 spectra being recorded for each interval over a 63-channel, pseudo-logarithmic energy scale. The first four spectra are measured with a fixed accumulation time of 64 ms in order to study short bursts.

Methods Table 3. Konus-*Wind* calibrations for GRB 200415A and GRB 051103

Burst	Det.	Inc. angle (deg)	G1 (keV)	G2 (keV)	G3 (keV)	PHA1 (keV)	PHA2 (keV)
GRB 200415A	S1	62.2	22–90	90–390	390–1600	28–1600	330–20000
GRB 051103	S2	70.8	17–70	70–300	300–1200	20–1170	240–14800

For this analysis we use a standard KW dead time (DT) correction procedure for light curves (with a DT of a few microseconds) and multichannel spectra (with a DT of ~ 42 microseconds).

Temporal analysis For the temporal analysis we used time histories from $T_0 - 0.512$ s to $T_0 + 0.512$ s in three energy bands: G1, G2, and G3 with a time resolution of 2 ms. The total burst duration T_{100} , and the T_{90} and T_{50} durations (the time intervals that contain 5% to 95% and 25% to 75% of the total burst count fluence, respectively⁵⁷), were calculated in this work using the light curve in the ~ 80 –1500 keV energy band (G2+G3). Burst start and end times in each band were calculated at the 5σ level with a method similar to that developed for BATSE⁵⁸. The background count rates, estimated using the data from $\sim T_0 - 2500$ s to $\sim T_0 - 150$ s, are 958.7 s^{-1} (G1), 349.5 s^{-1} (G2), and 223.0 s^{-1} (G3); and 1080.3 s^{-1} (G1), 394.0 s^{-1} (G2), and 135.5 s^{-1} (G3) for GRB 200415A and GRB 051103, respectively.

Spectral analysis For the bursts of interest we analysed both multichannel and three-channel KW energy spectra. The multichannel spectra accumulation intervals are presented in Extended Data Tables 2 and 3. The background multichannel spectra were extracted in the intervals from $T_0 + 8.448$ s to $T_0 + 491.776$ s and from $T_0 + 98.560$ s to $T_0 + 491.776$ for GRB 200415A and GRB 051103, respectively. The emission evolution at a finer time scale can be explored using three-channel spectra, constructed from the counts in the G1, G2, and G3 energy bands in the six intervals (Extended Data Tables 2 and 3). Details on KW three-channel spectral analysis can be found elsewhere²¹.

We performed the spectral analysis in XSPEC, version 12.10.1⁵⁹, using the following spectral models: a simple power law (PL), a custom exponential cutoff power-law (CPL) parametrized with peak of νF_ν spectrum and energy flux as the model normalization, the Band GRB function⁶⁰, a single blackbody (BB) function with the normalization proportional to the surface area, and a sum of CPL and BB functions (CPL+BB). The details of each model are presented below.

The power law model:

$$f_{\text{PL}} = A(E/E_n)^\alpha ; \quad (1)$$

the custom exponentially cutoff power law (CPL):

$$\begin{aligned} n(E) &= (E/E_n)^\alpha \exp(-E(2+\alpha)/E_p) \\ f_{\text{CPL}} &= F \times n(E) / \int_{E_{\min}}^{E_{\max}} n(E) E dE ; \end{aligned}$$

the Band function:

$$f_{\text{Band}} = A \begin{cases} (E/E_n)^\alpha \exp\left(-\frac{E(2+\alpha)}{E_p}\right), & E < (\alpha - \beta) \frac{E_p}{2+\alpha} \\ (E/E_n)^\beta \left[\frac{E_p(\alpha-\beta)}{E_n(2+\alpha)}\right]^{(\alpha-\beta)} \exp(\beta - \alpha), & E \geq (\alpha - \beta) \frac{E_p}{2+\alpha}, \end{cases}$$

where f is the photon spectrum, measured in photon $\text{cm}^{-2} \text{s}^{-1} \text{keV}^{-1}$, A is the model normalization, $E_n = 100 \text{ keV}$ is the pivot energy, E_p is the peak energy of the νF_ν spectrum, and F is the model energy flux in the $E_{\min} - E_{\max}$ energy band; α and β are the low-energy and high-energy photon indices, respectively. The single blackbody (BB) function is the `bbbodyrad` XSPEC model.

The Poisson data with Gaussian background statistic (PG-stat) was used in the model fitting process as a figure of merit to be minimized. The spectral channels were grouped to have a minimum of one count per channel to ensure the validity of the fit statistic. Since the CPL fit to a three-channel spectrum has zero degrees of freedom (and, in the case of convergence, PG-stat=0), we do not report the statistic for such fits. The 68% confidence intervals of the parameters were calculated using the command `steppar` in XSPEC.

A summary of constrained spectral fits with CPL, BB, and CPL+BB models is presented in Extended Data Tables 2 and 3. For both GRB 200415A and GRB 051103, the PL model failed to describe the spectra, with PG-stat/dof > 10 in all cases. Use of the Band GRB function does not constrain the high-energy photon index β for GRB 200415A spectra, and only marginally improves the CPL fit to the time-integrated spectrum of GRB 051103, with similar, within errors, E_p and α , and $\beta \sim -3$.

Burst energetics For both bursts, the total energy fluence S was derived using the 20 keV–10 MeV energy flux of the best-fit (CPL+BB) spectral model. Since the time-integrated spectrum accumulation interval differs from the T_{100} interval, a correction which accounts for the emission outside the time-integrated spectrum was introduced when calculating S .

The peak flux F_{peak} was calculated on the 4 ms scale using the energy flux of the best fit with CPL model to the three-channel spectrum at the peak count rate interval ($T_0 - 0.002$ s– $T_0 + 0.002$ s). We note, that the peak flux of GRB 051103 estimated in this work is a factor of ~ 2.5 lower than that reported from the previous analyses of KW and RHESSI data^{7,8}, which used wider spectral intervals and did not separate the relatively soft spectrum in the huge 4 ms spike ($E_p \sim 1.2$ MeV) and the considerably harder emission observed immediately after its falling edge ($E_p \sim 3$ MeV).

References for Methods

References

30. Meegan, C. *et al.* The Fermi Gamma-ray Burst Monitor. *Astrophys. J.* **702**, 791-804 (2009). [0908.0450](#).
31. Barthelmy, S. D. *et al.* The Burst Alert Telescope (BAT) on the SWIFT Midex Mission. *Space Sci. Rev.* **120**, 143-164 (2005). [astro-ph/0507410](#).
32. Rau, A. *et al.* The 1st INTEGRAL SPI-ACS gamma-ray burst catalogue. *Astron. Astrophys.* **438**, 1175-1183 (2005). [astro-ph/0504357](#).
33. Ubertini, P. *et al.* IBIS: The Imager on-board INTEGRAL. *Astron. Astrophys.* **411**, L131-L139 (2003).
34. Labanti, C. *et al.* The IBIS-PICsIT detector onboard INTEGRAL. *Astron. Astrophys.* **411**, L149-L152 (2003).
35. Boynton, W. V. *et al.* The Mars Odyssey Gamma-Ray Spectrometer Instrument Suite. *Space Sci. Rev.* **110**, 37-83 (2004).

36. Hurley, K. *et al.* Mars Odyssey Joins the Third Interplanetary Network. *Astrophys. J. Supp.* **164**, 124-129 (2006). [astro-ph/0508379](#).
37. Aptekar, R. L. *et al.* Konus-W Gamma-Ray Burst Experiment for the GGS Wind Spacecraft. *Space Sci. Rev.* **71**, 265-272 (1995).
38. Harten, R. & Clark, K. The Design Features of the GGS Wind and Polar Spacecraft. *Space Sci. Rev.* **71**, 23-40 (1995).
39. Neubert, T. The Atmosphere-Space Interactions Monitor (ASIM) for the International Space Station. *AGU Fall Meeting Abstracts* **2006**, AE42A-03 (2006).
40. The Fermi GBM Team GRB 200415A: Fermi GBM Final Real-time Localization. *GRB Coordinates Network* **27579**, 1 (2020).
41. Kunzweiler, F. *et al.* GRB 200415A: BALROG localization (Fermi Trigger 608633290 / GRB 200415367). *GRB Coordinates Network* **27580**, 1 (2020).
42. Goldstein, A. *et al.* Evaluation of Automated Fermi GBM Localizations of Gamma-Ray Bursts. *Astrophys. J.* **895**, 40 (2020). [1909.03006](#).
43. Burgess, J. M. *et al.* Awakening the BALROG: BAYesian Location Reconstruction Of GRBs. *Mon. Not. R. Astron. Soc.* **476**, 1427-1444 (2018).
44. Berlato, F. *et al.* Improved Fermi-GBM GRB Localizations Using BALROG. *Astrophys. J.* **873**, 60 (2019). [1902.01082](#).
45. Svinkin, D. *et al.* IPN triangulation of GRB 200415A (possible Magnetar Giant Flare in Sculptor Galaxy?). *GRB Coordinates Network* **27585**, 1 (2020).
46. Omodei, N. *et al.* GRB 200415A: Fermi-LAT detection. *GRB Coordinates Network* **27586**, 1 (2020).
47. Svinkin, D. *et al.* Improved IPN error box for GRB 200415A (consistent with the Sculptor Galaxy). *GRB Coordinates Network* **27595**, 1 (2020).
48. Omodei, N. *et al.* GRB 200415A: Fermi-LAT localization update. *GRB Coordinates Network* **27597**, 1 (2020).

49. Lipunov, V. *et al.* GRB 200415A: MASTER inspection and possible localisation. *GRB Coordinates Network* **27599**, 1 (2020).
50. Hurley, K. *et al.* The Interplanetary Network. *EAS Publications Series* **61**, 459-464 (2013).
51. Hurley, K. *et al.* The Interplanetary Network Supplement to the Fermi GBM Catalog of Cosmic Gamma-Ray Bursts. *Astrophys. J. Supp.* **207**, 39 (2013). [1301.3522](#).
52. Pal'shin, V. D. *et al.* Interplanetary Network Localizations of Konus Short Gamma-Ray Bursts. *Astrophys. J. Supp.* **207**, 38 (2013). [1301.3740](#).
53. Tohuvavohu, A. *et al.* Gamma-ray Urgent Archiver for Novel Opportunities (GUANO): Swift/BAT event data dumps on demand to enable sensitive sub-threshold GRB searches. *arXiv e-prints* **1**, arXiv:2005.01751 (2020). [2005.01751](#).
54. Hurley, K. *et al.* Precise Interplanetary Network Localization of the Bursting Pulsar GRO J1744-28. *Astrophys. J.* **537**, 953-957 (2000). [astro-ph/9912506](#).
55. Martin, D. C. *et al.* The Galaxy Evolution Explorer: A Space Ultraviolet Survey Mission. *Astrophys. J.* **619**, L1-L6 (2005). [astro-ph/0411302](#).
56. Gil de Paz, A. *et al.* The GALEX Ultraviolet Atlas of Nearby Galaxies. *Astrophys. J. Supp.* **173**, 185-255 (2007). [astro-ph/0606440](#).
57. Kouveliotou, C. *et al.* Identification of Two Classes of Gamma-Ray Bursts. *Astrophys. J.* **413**, L101 (1993).
58. Koshut, T. M. *et al.* Systematic Effects on Duration Measurements of Gamma-Ray Bursts. *Astrophys. J.* **463**, 570 (1996).
59. Arnaud, K. A. XSPEC: The First Ten Years. *Astronomical Society of the Pacific Conference Series* **101**, 17 (1996).
60. Band, D. *et al.* BATSE Observations of Gamma-Ray Burst Spectra. I. Spectral Diversity. *Astrophys. J.* **413**, 281 (1993).

Data Availability

Links to the *Wind* ephemeris and clock accuracy data are provided in the Methods section. The Konus-*Wind* lightcurve and spectral data are available at Ioffe web site <http://www.ioffe.ru/LEA/papers/SvinkinNat2020/data/>. The HEND lightcurve is available from the HEND team on reasonable request. The *Fermi*, *Swift*, and *INTEGRAL* data are freely available on-line.

Code availability

XSPEC is freely available on-line.

Acknowledgements

The authors thank Eric Burns for numerous useful discussions. The authors thank Oliver Roberts for reading the manuscript and providing useful comments. We thank Valentin Pal'shin for his considerable contribution to the Konus-*Wind* and IPN data analysis tools. A.B., P.U. and J.C.R. acknowledge the continuous support from the Italian Space Agency ASI via different agreements including the latest one, 2019-35-HH.0. The Konus-*Wind* experiment is supported by the Russian State Space Corporation ROSCOSMOS. The HEND experiment is supported by ROSCOSMOS and implemented as part of Gamma-Ray Spectrometer suite on NASA *Mars-Odyssey*. HEND data processing is funded by Ministry of Science and Higher Education of the Russian Federation, grant AAAA-A18-118012290370-6.

Author contributions statement

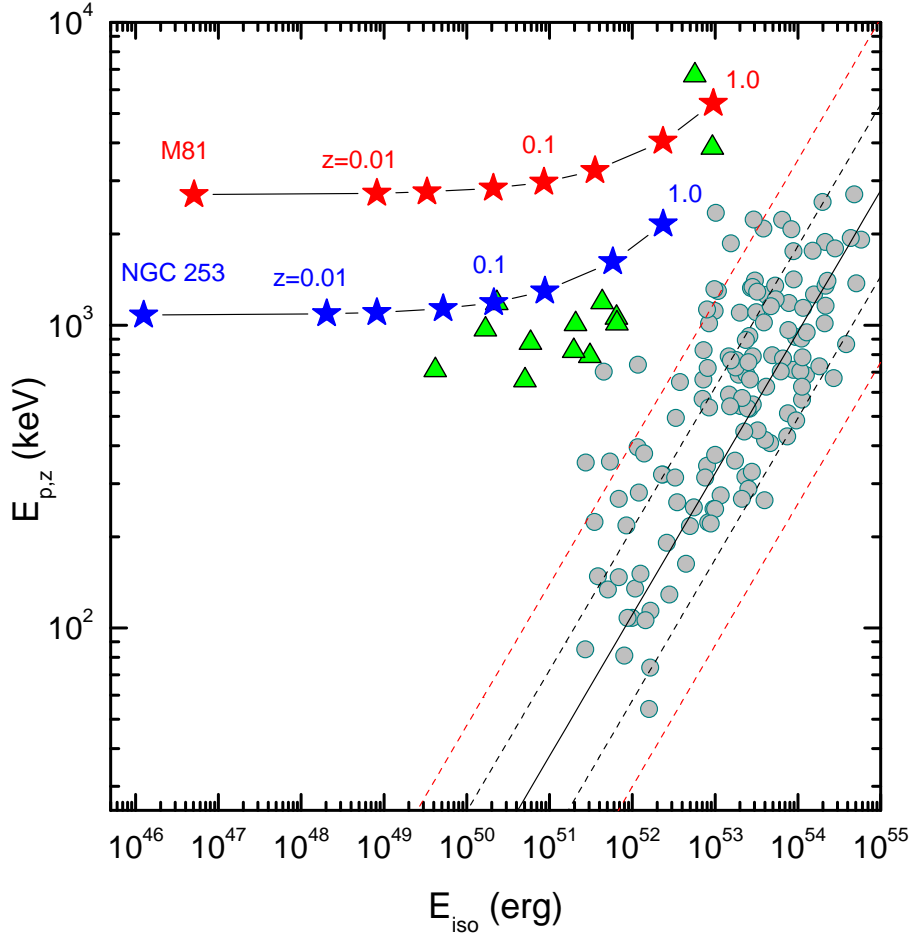
D.S. and K.H. performed the Interplanetary Network localization with the contributions of the Konus-*Wind* team (R.A., D.F., S.G., A.V.R., and T.L.C.); the Mars Odyssey (HEND and GRS) teams (I.M., D.G., A.K., M.L., A.S., W.B., C.W.F., K.P.H., H.E., and R.S.); the *Fermi*-GBM team (A.G., M.S.B., and C.W-H); the INTEGRAL (SPI-ACS and IBIS-PICsIT) teams (A.vK., X.Z., A.R., V.S., E.B., C.F., P.U., A.B., and J.C.R.), and the *Swift*-BAT team (S.B., J.C., H.K., and D.M.P.). D.F. and D.S. performed the Konus-*Wind* temporal and spectral data analysis with the contributions of A.L., A.V.R., A.T., and M.U. D.S., D.F. wrote and K.H. refined the manuscript. All authors provided comments on the paper.

Additional information

Correspondence and requests for materials should be addressed to Dmitry Svinkin (svinkin@mail.ioffe.ru).

Competing interests

The authors declare no competing financial interests.



Extended Data Figure 1. GRB 051103 (red stars) and GRB 200415A (blue stars) as possible cosmological GRBs at different redshifts ($0.01 < z < 1$). The Konus-Wind samples of short/hard and long GRBs with known redshifts²⁸ are shown by triangles and circles, respectively. The recent update²⁸ for the hardness-intensity relation in the cosmological rest frame ($E_{p,z}$ - E_{iso} , ‘Amati’ relation) is plotted with the solid line together with its 68% and 90% prediction intervals (dashed lines). Considering only its spectrum and energy fluence, GRB 200415A is consistent with the KW sample of short GRBs if at redshift $z \sim 0.05 - 1$. In the case of GRB 051103, the implied short GRB redshift is $z \sim 1$, and intrinsic $E_p \sim 5$ MeV.

Extended Data Table 1. Summary of GRB 200415A and GRB 051103 properties

Parameter	GRB 200415A	GRB 051103
Host galaxy (distance)	NGC 253 (3.5 Mpc)	M81/M82 group (3.6 Mpc)
Temporal properties		
T_{rise} (ms)	$\lesssim 2$	$\lesssim 4$
τ_{cr} (ms)	~ 50	~ 50
τ_{flux} (ms)	~ 30	~ 30
T_{100} (s)	0.138	0.324
T_{90} (s)	0.100 ± 0.014	0.138 ± 0.020
T_{50} (s)	0.048 ± 0.005	0.058 ± 0.004
Peak spectrum T_0 (-0.002 s, +0.002 s), CPL model		
CPL photon index α	$-0.59^{+0.17}_{-0.17}$	$-0.13^{+0.18}_{-0.17}$
CPL Peak energy E_p (keV)	1190^{+460}_{-240}	1250^{+590}_{-290}
Time-integrated spectrum T_0 (0, +0.192 s), CPL+BB model		
CPL photon index α	$-0.02^{+0.38}_{-0.25}$	$0.08^{+0.28}_{-0.19}$
CPL Peak energy E_p (keV)	1080^{+210}_{-150}	2690^{+210}_{-180}
Blackbody temperature kT (keV)	99^{+37}_{-33}	107^{+11}_{-10}
Blackbody radius R (km)	23^{+16}_{-9} (@3.5 Mpc)	37^{+6}_{-6} (@3.6 Mpc)
Blackbody contribution to flux	$\sim 14\%$	$\sim 9\%$
Peak energy fluxes ($\text{erg cm}^{-2} \text{s}^{-1}$), in the 20 keV–10 MeV band		
4 ms scale, T_0 (-0.002 s, +0.002 s)	$9.6^{+3.2}_{-1.6} \times 10^{-4}$	$11.5^{+5.2}_{-2.4} \times 10^{-4}$
16 ms scale, T_0 (-0.002 s, +0.014 s)	$1.11^{+0.21}_{-0.14} \times 10^{-4}$	$8.98^{+5.79}_{-2.36} \times 10^{-4}$
64 ms scale, T_0 (-0.002 s, +0.062 s)	$0.43^{+0.07}_{-0.05} \times 10^{-4}$	$4.38^{+1.61}_{-0.88} \times 10^{-4}$
Energy fluences (erg cm^{-2}), in the 20 keV–10 MeV band		
Initial spike	$3.86^{+1.27}_{-0.66} \times 10^{-6}$ T_0 (-0.002 s, +0.002 s)	$4.61^{+2.09}_{-0.96} \times 10^{-6}$ T_0 (-0.002 s, +0.002 s)
Total	$8.5^{+1.2}_{-1.0} \times 10^{-6}$ T_0 (-0.004 s, +0.192 s)	$34.3^{+4.0}_{-2.0} \times 10^{-6}$ T_0 (-0.006 s, +0.192 s)
Flare energetics, in the 20 keV–10 MeV band		
L_{iso} , 4 ms scale (erg s^{-1})	$\sim 1.4 \times 10^{48}$	$\sim 1.8 \times 10^{48}$
E_{iso} (erg)	$\sim 1.3 \times 10^{46}$	$\sim 5.3 \times 10^{46}$
KW maximal detection distance (Mpc)	~ 13.5	~ 15.8

Extended Data Table 2. GRB 200415A spectral fits

Time interval (s)	model	α	E_p (keV)	kT (keV)	R (km)	Flux (20 keV–10 MeV) (10^{-6} erg cm $^{-2}$ s $^{-1}$)	PGstat/dof
Three-channel spectra							
-0.004 – -0.002	CPL	$-0.28^{+0.58}_{-0.49}$	520^{+390}_{-140}	–	–	81^{+35}_{-17}	–
-0.002 – 0.002	CPL	$-0.59^{+0.17}_{-0.17}$	1190^{+460}_{-240}	–	–	960^{+250}_{-130}	–
0.002 – 0.032	CPL	$0.30^{+0.29}_{-0.25}$	980^{+230}_{-150}	–	–	111^{+21}_{-14}	–
0.032 – 0.064	CPL	$0.16^{+0.29}_{-0.26}$	710^{+160}_{-100}	–	–	43^{+7}_{-5}	–
0.064 – 0.096	CPL	$0.44^{+0.60}_{-0.45}$	496^{+84}_{-56}	–	–	$19.3^{+2.9}_{-2.2}$	–
0.096 – 0.128	BB	–	–	73^{+8}_{-7}	54^{+21}_{-14}	$6.8^{+1.1}_{-0.9}$	0.5/1
Multichannel spectra							
0.000 – 0.064	CPL	$0.12^{+0.15}_{-0.14}$	1066^{+91}_{-79}	–	–	$85.4^{+6.9}_{-6.3}$	55/64
0.064 – 0.128	CPL	$0.39^{+0.39}_{-0.33}$	458^{+78}_{-57}	–	–	$12.5^{+2.2}_{-1.8}$	49/47
0.128 – 0.192	BB	–	–	71^{+22}_{-15}	$26^{+12}_{-9.0}$	$1.47^{+0.57}_{-0.42}$	22/31
0.000 – 0.192	CPL	$0.01^{+0.12}_{-0.12}$	887^{+76}_{-67}	–	–	$32.3^{+2.4}_{-2.3}$	67/75
	CPL+BB	$-0.02^{+0.38}_{-0.25}$	1080^{+210}_{-150}	99^{+31}_{-32}	$23^{+16}_{-9.0}$	$33.3^{+5.1}_{-5.0}$	63/73

Extended Data Table 3. GRB 051103 spectral fits

Time interval (s)	model	α	E_p (keV)	kT (keV)	R (km)	Flux (20 keV–10 MeV) (10^{-6} erg cm $^{-2}$ s $^{-1}$)	PGstat/dof
Three-channel spectra							
-0.004 – -0.002	CPL	$-0.32^{+0.43}_{-0.36}$	1380^{+9850}_{-640}	–	–	207^{+817}_{-84}	–
-0.002 – 0.002	CPL	$-0.13^{+0.18}_{-0.17}$	1250^{+590}_{-290}	–	–	1150^{+520}_{-240}	–
0.002 – 0.032	CPL	$0.20^{+0.18}_{-0.16}$	3620^{+7980}_{-1540}	–	–	940^{+1370}_{-430}	–
0.032 – 0.064	CPL	$0.64^{+0.73}_{-0.43}$	930^{+350}_{-240}	–	–	116^{+41}_{-20}	–
0.064 – 0.096	CPL	$0.28^{+0.40}_{-0.31}$	607^{+153}_{-97}	–	–	42^{+7}_{-5}	–
0.096 – 0.128	BB	–	–	93^{+8}_{-7}	47^{+7}_{-7}	$13.1^{+1.6}_{-1.5}$	0.8/1
Multichannel spectra							
0.000 – 0.064	CPL	$-0.02^{+0.08}_{-0.08}$	2570^{+160}_{-150}	–	–	444^{+27}_{-25}	93/77
	CPL+BB	$0.39^{+0.34}_{-0.24}$	2790^{+200}_{-150}	129^{+22}_{-18}	$35.5^{+8.1}_{-8.9}$	444^{+32}_{-31}	83/75
0.064 – 0.128	CPL	$0.47^{+0.25}_{-0.23}$	565^{+53}_{-45}	–	–	$34.2^{+3.1}_{-2.8}$	57/58
0.128 – 0.192	CPL	$0.66^{+1.30}_{-0.87}$	320^{+119}_{-67}	–	–	$5.5^{+1.0}_{-0.9}$	29/43
	BB	–	–	75^{+9}_{-8}	45^{+9}_{-8}	$5.1^{+0.8}_{-0.7}$	30/44
0.000 – 0.192	CPL	$-0.30^{+0.06}_{-0.06}$	2300^{+150}_{-140}	–	–	162^{+9}_{-9}	127/85
	CPL+BB	$0.08^{+0.28}_{-0.19}$	2690^{+210}_{-180}	107^{+11}_{-10}	36^{+6}_{-7}	162^{+11}_{-10}	98/83